Employing the Generative Adversarial Networks (GAN) for Reliability Assessment of Converters

Davoodi, Amirali; Peyghami, Saeed; Yang, Yongheng; Dragičević, Tomislav; Blaabjerg, Frede

Published in:
2021 IEEE Energy Conversion Congress and Exposition (ECCE)

DOI (link to publication from Publisher):
10.1109/ECCE47101.2021.9595614

Publication date:
2021

Document Version
Accepted author manuscript, peer reviewed version

Employing the Generative Adversarial Networks (GAN) for Reliability Assessment of Converters

Amirali Davoodi[1], Saeed Peyghami[1], Yongheng Yang[2], Tomislav Dragičević[3], and Frede Blaabjerg[1]
[1] Department of Energy Technology, Aalborg University, Aalborg, Denmark
[2] College of Electrical Engineering, Zhejiang University, Hangzhou, China
[3] Department of Electrical Engineering, Technical University of Denmark, Copenhagen, Denmark
amirali.davoodi@et.aau.dk

***Abstract*—Mission profiles are widely used for the reliability analysis of power converters. Typically, to assess the converter reliability, long-term (e.g., one year) mission profiles are adopted, and it is assumed that the profiles will be repeated in future years. However, due to mission profile uncertainties, the assumption can introduce considerable errors in the estimated reliability. In this paper, the errors introduced by the above assumption are studied in detail. Furthermore, to tackle this challenge, the paper proposes using the Generative Adversarial Networks (GAN) to generate unique mission profile scenarios that capture the temporal and probabilistic properties of the real profiles. In this regard, the effectiveness of using the GAN-generated profiles to improve the accuracy of the estimated reliability is demonstrated.**

Keywords—Power Electronics, reliability, Generative Adversarial Networks, GAN, mission profiles, power converters

I. INTRODUCTION

Nowadays, power electronic converters are used in a wide range of grid applications – e.g., PhotoVoltaic (PV) and wind power generation systems [1]. Due to the pivotal role of power converters in many applications, their failures can have many consequences. For example, in the case of converter failure in wind and PV applications, economic losses are inevitable due to the maintenance and the energy not produced in the downtime. Notably, in some field studies of failures in PV and wind applications [2], [3], power converters are reported as one of the main sources of unreliability. Therefore, the reliability of converters is of importance and should be assessed properly in order to avoid such consequences.

Using handbooks is a conventional way of reliability assessment for power converters. For example, the reliability assessment of a modular multilevel converter was done in [4] based on the MIL-HDBK-217F [5]. Similarly, in [6], the MIL-HDBK-217 is used for the reliability assessment of DC-DC boost converters. However, the main drawback of using this handbook for reliability assessment is ignoring the mission profiles. In other words, a converter that is operating in a high-loading condition is more likely to fail compared to the one that usually works in a low-load condition. This fact is, however, ignored when using the MIL-HDBK-217F. To address this problem, [7] uses the FIDES guide [8] for the reliability assessment of a PV system. Nevertheless, since constant failure rates are calculated for devices, this approach neglects the wear-out failures and the aging of power devices, while it is a key contributing factor in the overall failures of power converters [9]. As a result, the concept of model-based and mission-profile-based reliability assessment – also known as Stress-Strength Analysis (SSA) [10] – has attracted much attention recently. In this regard, an optimal reliability-oriented design of a PV inverter was done in [11] by employing this concept and Artificial Intelligence (AI). Also, in [12], the lifetime of power semiconductors is predicted by using the SSA, and the results are validated through experimental wear-out tests.

As mentioned earlier, mission profiles are one of the main components of the SSA. During the SSA process, typically, long-term mission profiles (e.g., one year) are studied, and it is assumed that the same mission profile will be repeated exactly in future years. However, in reality, the mission profiles that will take place in the future can be different compared to the considered ones. Consequently, these differences, which are caused due to the mission profile uncertainties, will introduce errors to the estimated reliability, which is not favorable. To tackle this challenge, this paper proposes to generate unique and realistic mission profile scenarios based on the existing mission profile. Also, the number of generated mission profile scenarios must be sufficiently large to emulate and cover most of the possible scenarios, which may happen in the future. In other words, generated profiles must display sufficient diversity and variations (so that they can represent most of the scenarios that may happen in the future) while keeping the similarities and intrinsic features of the existing mission profiles (being as realistic as possible).

To generate a large number of unique and realistic profiles based on the existing profile, several techniques can be employed. For instance, time series analysis techniques such as Auto Regressive Moving Average (ARMA) [13] are an option. However, these approaches are likely to overfit or misidentify the patterns and need a large number of historical profiles to express enough diversity in the generated profiles [14]. Also, probabilistic methods such as Monte Carlo Simulation (MCS) or Latin Hypercube Sampling (LHS) can be helpful [15]. Nonetheless, these techniques often require a large number of historical data to reconstruct the original distribution. In addition, they cannot properly model the temporal properties of the historical profiles [14].

Considering the above reasons, this paper utilizes the Machine Learning (ML) concept of Generating Adversarial Networks (GAN) [16] to perform the mission profile scenario generation task. The GAN is a data-driven and model-free approach, which obviates the shortcomings of using ARMA, MCS, and LHS, and thereby being suitable for mission profile scenario generation. Notably, the GAN incorporates two Deep Neural Networks (DNNs) in its architecture, which are trained simultaneously, as will be explained in Section III. Additionally, once the DNNs are trained according to the existing profiles, new mission profiles can be generated fast. This enables generating a large number of profiles to capture

This work was supported by THE VELUX FONDEN under the VILLUM Investigator grant for the REPEPS project at Aalborg University.

enough diversity to cover all the possibilities that may be experienced in the future. Furthermore, the generated scenarios can be evaluated in terms of uniqueness and being realistic by performing several tests on their Cumulative Distribution Function (CDF), Power Spectral Density (PSD), and temporal properties. Accordingly, by employing the GAN, the mission profile uncertainty can be incorporated effectively into the reliability assessment, thereby improving its accuracy.

The rest of the paper is organized as follows. Section II explains the steps to realize the mission-profile- and model-based reliability assessment by using the SSA. Section III discusses the principles of GAN and employing it for mission profile generation. Section IV presents the results of the generated scenarios and does the reliability assessment of a case study PV inverter. Finally, the conclusions are drawn in Section V.

II. Model-Based Reliability Assessment

An overview of the model-based reliability assessment procedure, considering the mission profiles of power converters, is illustrated in Fig. 1, which will be discussed in this section. In this regard, to assess the reliability of a converter, several steps, i.e., electro-thermal modeling, damage estimation, Monte Carlo Simulation (MCS), and Reliability Block Diagram (RBD), must be taken, which are elaborated here.

A. Electro-Thermal Modeling

Power semiconductors are one of the key sources of failures in power converters [17]. Furthermore, temperature and its cycling are known as the main factor in triggering wear-out failures in power semiconductors. Therefore, in order to estimate the converter reliability, it is necessary to have the temperature profile of the semiconductors. In this regard, the temperature of a power semiconductor is mainly determined by its power losses. Notably, the power losses are a function of the mission profiles (e.g., semiconductor's voltage and current profile), and they can cause large temperature fluctuations. Hence, electro-thermal modeling is an inseparable part of translating the mission profiles to the temperature profile of the components. If the Insulated-Gate Bipolar Transistor (IGBT) output characteristic can be linearized, the relationship between the saturation voltage, V_{CEsat}, and the current, i_C, can be written as

$$V_{CEsat} = V_{CE0} + r_{CE}.i_C \tag{1}$$

where V_{CE0} and r_{CE} can be obtained by curve-fitting the voltage-current curve presented in the IGBT datasheets. Subsequently, for an IGBT-based three-phase full-bridge converter with the sinusoidal pulse width modulation, the conduction and switching losses of the transistor can be calculated as [18]

$$P_C = (\frac{1}{2\pi} + \frac{m\cos\varphi}{8})V_{CE0}I_1 + (\frac{1}{8} + \frac{m\cos\varphi}{3\pi})r_{CE}I_1^2 \tag{2}$$

$$P_S = f_{sw}(E_{on} + E_{off})\frac{I_1}{\pi I_{ref}}(\frac{V_{DC}}{V_{ref}})^{K_V}(1 + \alpha_{E_{SW}}(T_j - T_{ref})) \tag{3}$$

where f_{sw} is the switching frequency, I_1 is the amplitude of the fundamental component of the inverter output current, m is the modulation index, α_{Esw} is the temperature coefficient of the switching losses, I_{ref}, V_{ref}, and T_{ref} are the reference values for current, voltage, and temperature in the IGBT datasheet, and E_{on} and E_{off} are turn-on and turn-off energy losses per pulse.

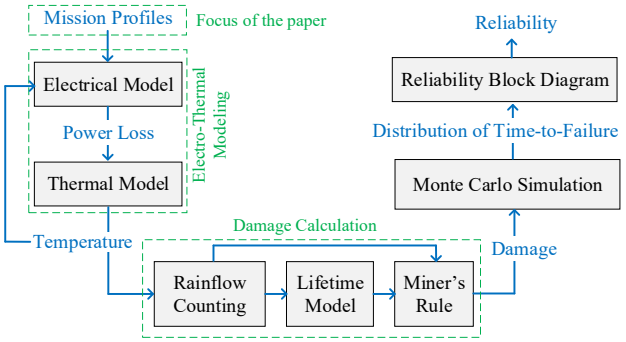

Fig. 1. Procedure for model-based and mission profile-based reliability assessment of power converters.

As a result, the junction temperature of the IGBT during the steady-state operation can be found from

$$T_j = T_a + (P_C + P_S).\sum R_{th} \tag{4}$$

where ΣR_{th} is the sum of the thermal resistance in the thermal model of the IGBT.

It is worth mentioning that for a PV inverter application, the Solar Irradiance (SI) and ambient temperature, i.e., SI and T_a, must be translated into the inverter input power and voltage through modeling the PV panels by either simulations or by using the equations presented in [19].

B. Damage Calculation

Once the IGBT junction temperature profile is obtained from the electro-thermal modeling, a counting algorithm, e.g., the rainflow counting method, can be applied to it. As a result, the junction temperature profile would be classified into several classes, where for each class, the number of occurrences, n, the range, ΔT_j, the maximum, T_{jmax}, and the on-time, t_{on}, are acquired.

Moreover, one of the widely-used lifetime models for IGBTs can be written as [10]

$$N_f = A\Delta T_j^{\beta_1}\exp(\frac{\beta_2}{T_{j\max} + 273})(\frac{t_{on}}{1.5})^{\beta_3} \tag{5}$$

where N_f is the number of cycles to failure. Also, as mentioned earlier, ΔT_j, T_{jmax}, and t_{on} are acquired from the rainflow counting algorithm. Other parameters of the lifetime model can be provided by the manufacturer [20] or obtained from the temperature cycling test in the laboratory [21]. Subsequently, the accumulated damage to the IGBT can be calculated from the Miner's rule as

$$D_{IGBT} = \sum_{i=1}^{K}\frac{n_i}{N_{fi}} \tag{6}$$

where n_i and N_{fi} are the number of occurrences (from the rainflow counting algorithm) and number of cycles to failure (from (5)) for the i^{th} class, and K is the total number of classes. It should be mentioned that the damage denotes the proportion of the lifetime of the IGBT, which is consumed every year.

C. Monte Carlo Simulation

Due to the small inevitable variations during the manufacturing process of devices, in reality, the IGBTs have slightly different characteristics and tolerances, which introduces uncertainties to the electro-thermal modeling.

Also, the lifetime model parameters come from a limited number of tests on a limited number of IGBTs, which causes uncertainties in the model parameters. Therefore, the damage to different IGBTs can be slightly different, which must be taken into account. This fact is considered by performing an MCS, where a Probability Density Function (PDF) – typically normal distribution – is assumed for the lifetime model and electro-thermal model parameters, rather than a constant value. Therefore, a PDF would be obtained for the accumulated damage D_{IGBT}, and not only a constant value. Finally, for a single IGBT, the PDF of time-to-failure, $f(t)$, can be calculated by finding the distribution of $1/D_{IGBT}$.

D. Reliability Block Diagram

When the PDF of the time-to-failure is calculated for a single IGBT, the converter-level reliability can be obtained by using the RBD. In the RBD of the above-mentioned converter topology, all IGBTs are in series from the reliability point of view. In this case, the converter-level reliability can be calculated by

$$R(t) = \prod_{i=1}^{6} (1 - \int_{0}^{t} f_i(\tau) d\tau) . \quad (7)$$

where $f_i(.)$ is the PDF of time-to-failure for the i^{th} IGBT obtained based on Fig. 1, and t is time. It is worth mentioning that diodes and other components of the power converter can be incorporated into the analysis with a similar approach if needed. If the PDF of time-to-failure for all IGBTs are assumed to be identical and equal to $f(t)$, then $R(t) = (1 - \int_{0}^{t} f_i(\tau) d\tau)^6$.

III. Application of the GAN to Address the Mission Profile Uncertainties

In practice, due to the uncertainty of mission profiles, e.g., the Solar Irradiance (SI) profile, semiconductors will experience different mission profiles and junction temperature profiles at different years in the future. Thus, this mission profile uncertainty must be considered when assessing the converter reliability to avoid unrealistic results. To tackle this challenge, this paper proposes generating a sufficient number of mission profiles that could potentially occur to the system in the future. Each of the generated mission profiles must be distinct, while capturing all the instantaneous variations and diurnal patterns existing in the SI. In other words, the generated mission profiles must have the same visual, statistical, and temporal properties of the historical data. Considering all these properties and by generating a decent number of mission profiles, it can be ensured that most of the possible variations of junction temperature (i.e., ΔT_j, which is the most influential factor in the wear-out failures) are covered in the reliability assessment. More specifically, each mission profile will result in a different lifetime consumption, and when a large number (considering the appropriate stopping criteria) of realistic scenarios are considered, the mission profile uncertainty is included in the analysis naturally. It is worth mentioning that the generated mission profiles can be validated by doing several tests on their Power Spectral Density (PSD), Cumulative Distribution Function (CDF), and other temporal and statistical properties, which will be elaborated in the next section.

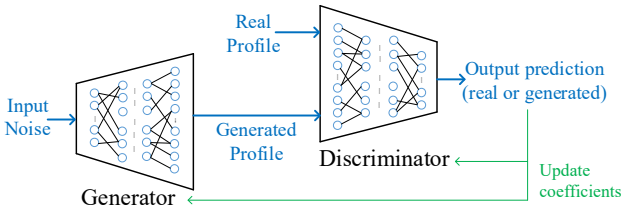

Fig. 2. Overall architecture of the Generative Adversarial Networks (GAN) and its training process.

Since this paper uses the GAN to generate realistic mission profile scenarios, this section explains the basic principles of the GAN and its training process. The overall architecture of the GAN is shown in Fig. 2. In the GAN, two DNNs are used – one for producing the nonlinear relationships (generator) and the other for the classification (discriminator). In fact, there is a game between the generator and discriminator, where the generator tries to generate data as realistic as possible, which is not distinguishable from the real data by the discriminator. The coefficients of the generator and discriminator DNNs are updated accordingly during each training epoch. According to the game theory, at the Nash equilibrium point, the generator is able to reconstruct the distribution of real data and generate data such that the discriminator cannot identify the difference between them and real data [14]. As a result, the final generated data are as realistic as possible when the equilibrium point is achieved. From Fig. 2, the input to the generator is Gaussian noise, which is transformed into the generated data after passing through the DNN, aiming at reconstructing the same statistical and temporal properties of the real data. The generated data in addition to the real data are the inputs of the discriminator, where the DNN tries to classify them. The coefficients of the generator and the discriminator are updated based on their success in their corresponding role.

This part will explain how the GAN is employed for generating mission profiles, where the objectives and loss functions are formulated, and the training process is elaborated. Consider that the real data (time series) are indexed by time such that $t = 1, 2, \ldots, T$. Thus, each point can be represented by x^t, where $t \in T$. Also, assume that P_X is the distribution of real data, which is unknown. In addition, z is a noise vector input sampled from a Gaussian distribution P_Z – that is, $Z \sim P_Z$. From a mathematical perspective, the GAN training process aims at training the generator and discriminator such that any random sample z drawn from P_Z follows P_X. If G is the generator function whose coefficients are $\theta^{(G)}$, it can be written as $G(\,.\,;\theta^{(G)})$. Similarly, D, the discriminator function whose coefficients are characterized by $\theta^{(D)}$ can be written as $D(\,.\,;\theta^{(D)})$. Given that Z is a random variable from P_Z, $G(\,.\,;\theta^{(G)})$ can be called another random variable following the distribution of P_G. The inputs to the discriminator are real and generated samples, and its output is p_{real}, which denotes to what degree the inputs belong to P_X, which can be written as

$$p_{real} = D(x;\theta^{(D)}) \quad (8)$$

where x belongs to P_{data} or P_Z. To identify Px from P_G, the difference between E[$D(X)$] and E[$D(G(Z))$] must be maximized. To simultaneously train the generator and discriminator, their corresponding loss functions L_G and L_D must be defined, and a game value function $V(G, D)$ is

required. According to [22], the loss functions can be written as

$$L_G = -\mathrm{E}_Z[D(G(Z))] \quad (9)$$

$$L_D = -\mathrm{E}_X[D(X)] + \mathrm{E}_Z[D(G(Z))]. \quad (10)$$

where G is the generator function, D is the discriminator function, Z is the random noise input, X is the historical data input, and E[.] denotes the expected value operator. By using the game value function $V(G, D)$, the above equations can be composed to make a two-player minimax game as [14]

$$\min_{\theta^{(G)}} \max_{\theta^{(D)}} V(G,D) = \mathrm{E}_X[D(X)] - \mathrm{E}_Z[D(G(Z))]. \quad (11)$$

At the beginning of the training, the data generated by the generator $G(z)$ is very different from P_X, which results in a small value for L_D and large values of L_G and $V(G, D)$. Over the training process, the value of L_G decreases, while L_D increases, until the optimal solution is reached and the generated data are not distinguishable from the real data. It is worth mentioning that the Wasserstein distance [22] is used as a criterion to check whether the optimal solution is reached.

IV. Case Study and Results

In this section, the above problem, in addition to the proposed solution, will be studied elaborately by assessing the reliability of a case study power converter. The schematic of the studied power electronic system is shown in Fig. 3. F3L25R12W1T4_B27 is selected as the IGBT module, whose lifetime parameters, presented in Table I, can be obtained from the data provided in [20]. The number of series- and parallel-connected panels in each of the arrays shown in Fig. 3 are 20 and 3, respectively, where BP365 65W is selected as the PV panel [23]. Other system parameters are presented in Tables II and III. It should be noted that, in this case study, the reliability of the PV inverter considering the IGBT failures will be studied.

An annual profile of the solar irradiance for the year 2007 at Las Vegas, NV, is presented in Fig. 4 [24]. Also, for the same location, the solar irradiance profile for week #30 at the years 2007, 2009, and 2014 are as shown in Fig. 5. As it can be seen in Fig. 5, the mission profiles may vary considerably from year to year. Therefore, the assumption that one mission profile is repeated every year might introduce some errors to the reliability estimation. To illustrate the errors introduced by this assumption, reliability of the case study shown in Fig. 3 is calculated based on the yearly solar irradiance profiles of 2007, 2009, and 2014, according to the SSA method explained in Section II. As a result, three reliability curves are obtained based on the annual profiles, as depicted in Fig. 6. As shown in Fig. 6, the estimated converter reliability significantly depends on the year that is selected as a mission

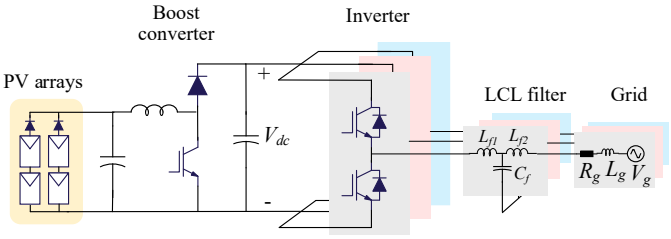

Fig. 3. Schematics of a double-stage PV system for the case study, including, the PV arrays, boost converter, PV inverter, LCL filter, and grid model.

TABLE I. Parameters of the IGBT Module Lifetime Model Given in (5)

Lifetime parameter	Value
A	8.3255×10^{14}
β_1	-7.01
β_2	2553
β_3	-0.3

TABLE II. Inverter Parameters For the System Shown in Fig. 3

Parameter	Value
V_{dc}	800 (V)
f_{sw}	2500 (Hz)
L_{1f}	3.5 (mH)
L_{2f}	0.5 (mH)
C_f	22 (μF)

TABLE III. Grid Parameters for the System Shown in Fig. 3

Parameter	Value
V_g	230 (V)
f_g	50 (Hz)
R_g	0.5 (Ω)
L_g	1 (mH)

profile. For instance, if the mission profile of 2007 was selected, the B_{10} lifetime is roughly 22 years for the converter, whereas selecting the profile of 2009 would lead to an estimation of approximately 12 years for the B_{10} lifetime.

A similar analysis was performed on the case study considering 14 different mission profiles from 2007 to 2020, where the annual damage to the IGBT was calculated from (6). The annual damage to the IGBTs is presented in Fig. 7, where it can be seen that the stress of the IGBTs varies from year to year, and accordingly, the annual damage can vary significantly. For instance, the annual damage in the year 2007 is 45% smaller than that of year 2009. Thus, these

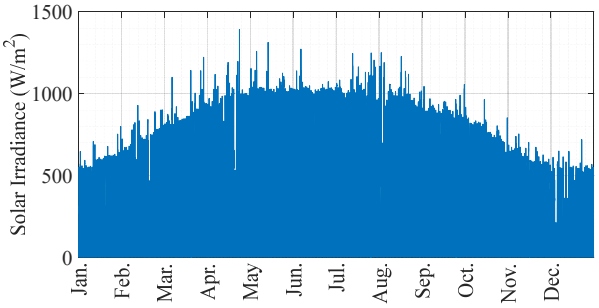

Fig. 4. Annual solar irradiance profile of Las Vegas, NV in 2007 [24].

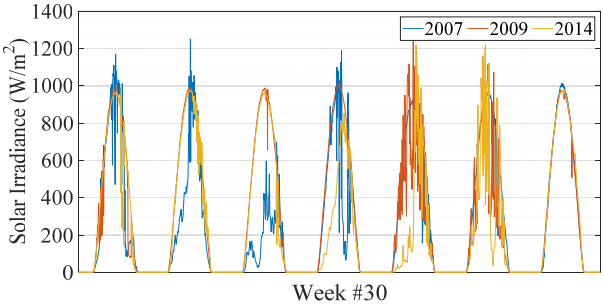

Fig. 5. Solar irradiance profile of week #30 at years 2007, 2009, and 2014.

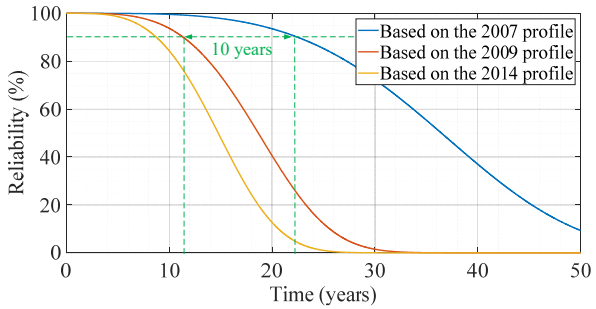

Fig. 6. Reliability of the converter considering different years of mission profiles – 2007, 2009, and 2014.

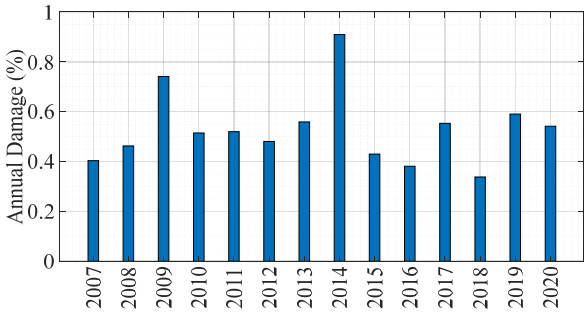

Fig. 7. Distribution of damage to the IGBTs for different years of mission profiles (historical data).

results suggest that the mission profile uncertainties can lead to significant errors in the reliability estimation if it is not taken into account.

To model these uncertainties, several mission profile scenarios are generated by using the GAN, as explained in Section III, where 150 mission profiles were generated by training it. A week of the generated profiles is illustrated together with the real profiles in Fig. 8. As it can be seen in Fig. 8, while they are unique and distinct, the generated profiles resemble the real profiles to a great extent, such that they are not distinguishable visually.

To further study the generated profiles, the average solar irradiance of the generated profiles in different months of a year is calculated and compared to that of the real profiles, as shown in Fig. 9. From Fig. 9, it can be seen that the values of the real and generated profiles match well in all months, indicating a good agreement between the temporal and probabilistic properties of the real and generated profiles.

In addition, the CDFs of the daytime solar irradiance in July and December are extracted based on both the real and generated profiles. The extracted CDFs are shown in Fig. 10, where the CDF of the generated profiles follows the CDF of the real profiles. This match suggests that, although the generated profiles are unique and different, they preserve the main statistical and temporal properties of the real profiles.

Moreover, the PSD of the generated and real profiles are extracted and plotted in Fig. 11. Notably, the PSD calculates the spectral power distribution that is present in each frequency band (appropriate for comparing the temporal properties). Therefore, the match between the PSD of real and generated profiles shows that the generated profiles also capture the temporal properties of the real profiles.

Based on the results presented in Fig. 7, the average annual damage to each IGBT from 2007 to 2020 is 0.53. However, if the reliability assessment was done only based on the mission profile of 2007, the annual damage would be 0.40, which indicates a 25% error. Nevertheless, when the reliability assessment is done based on the 150 GAN-generated mission profiles, the average annual damage will be 0.54, which matches 0.53 extracted before based on the real profiles from 2007 to 2020. In addition, the reliability curve of the inverter is extracted based on the 2007-2020

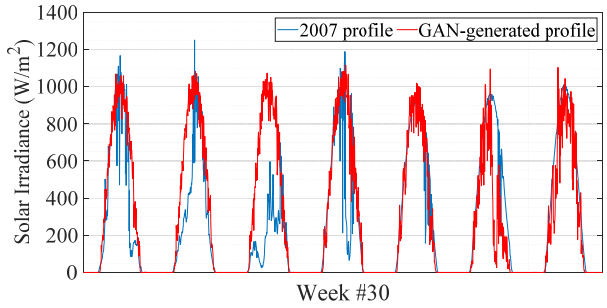

Fig. 8. Comparison of the time series of the real and generated profiles of solar irradiance.

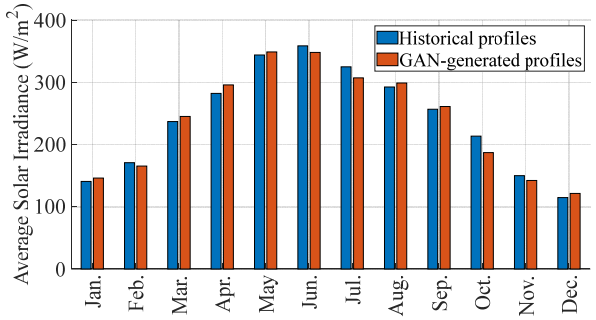

Fig. 9. Average solar irradiance in different months – a comparison between the historical and generated profiles using the GAN.

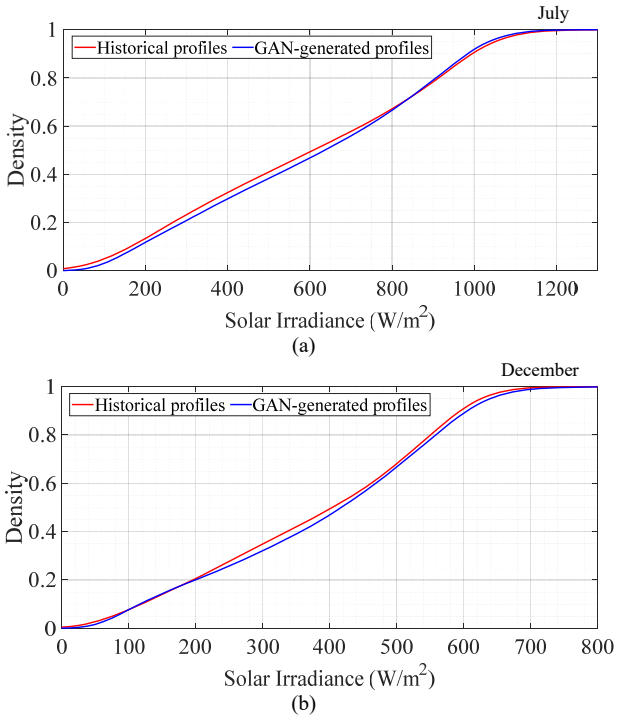

Fig. 10. CDF (Cumulative Distribution Function) of the daytime solar irradiance from the generated and historical profiles: (a) July and (b) December.

profiles, GAN-generated profiles, and 2007 profile only,

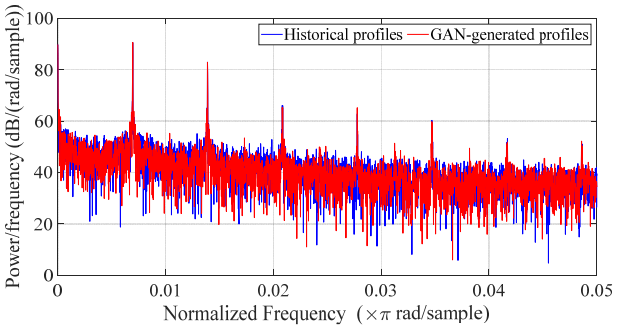

Fig. 11. PSD (Power Spectral Density) of the daytime solar irradiance from the generated and historical profiles.

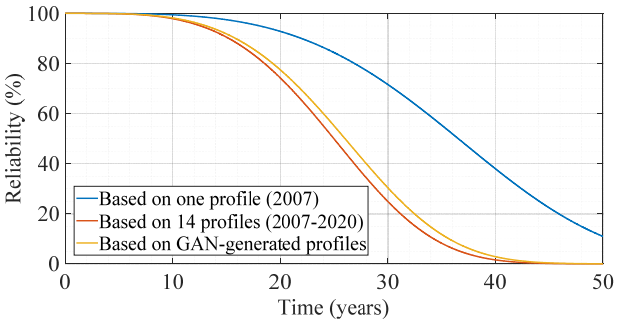

Fig. 12. Comparison of the estimated reliability from GAN-generated profiles and historical profiles.

where the results are shown in Fig. 12. As presented in Fig. 12, the curve extracted based on only the profile of 2007 does not follow the real value accurately, thereby introducing errors. In contrast, the reliability curves from the GAN-generated profiles as well as the 2007-2020 profiles match well, which confirms the effectiveness of using the GAN-generated profiles in reducing the sensitivity of the estimated reliability to the mission profile uncertainties, and thereby improving the accuracy of reliability assessment.

V. Conclusion

In the model-based reliability assessment methodology, the mission profiles play a key role. Typically, for the reliability assessment of converters, one year of mission profile is selected, and it is assumed that the same profile will be repeated in future years. However, due to the mission profile uncertainties, this assumption can introduce errors to the estimated reliability. The impact of mission profile uncertainties on the accuracy of the estimated reliability and damage was studied in this paper. It was shown that the damage of different years can be different – for example the damage in 2007 was 45% smaller than that of 2009. Additionally, the B_{10} lifetime estimated based on the 2007 profile was 10 years larger than that resulted from the 2009 profile. To consider these uncertainties, this paper proposed using Generative Adversarial Networks (GAN) to generate unique mission profile scenarios that have the temporal and probabilistic properties of the real profiles. In this regard, 150 mission profiles were generated by using the GAN. The generated profiles were compared with real profiles in terms of Cumulative Distribution Functions (CDFs), Power Spectral Densities (PSDs) and monthly average, where a good match was found between them. Subsequently, the reliability of a case study was assessed based on the 150 generated profiles as well as the real profiles from 2007-2020. As a result, the average annual damage from the generated profiles was 0.54, while this value was 0.53 for the profiles from 2007-2020. When only the mission profile of 2007 was used, the annual damage of 0.40 was obtained, which shows a 25% error compared to the results based on 2007-2020. Also, the reliability curves of the generated profiles matched the one obtained from 2007-2020 profiles. Therefore, using the GAN could assist the accuracy of the estimated reliability by considering the uncertainties of mission profiles over years.

References

[1] F. Blaabjerg, Y. Yang, D. Yang, and X. Wang, "Distributed power-generation systems and protection," *Proc. of the IEEE*, vol. 105, no. 7, pp. 1311–1331, Jul. 2017.

[2] A. Golnas, "PV system reliability: an operator's perspective," *IEEE J. Photovoltaics*, vol. 3, no. 1, pp. 416–421, Jan. 2013.

[3] Y. Lin, L. Tu, H. Liu, and W. Li, "Fault analysis of wind turbines in China," *Renew. Sustain. Energy Rev.*, vol. 55, pp. 482–490, Mar. 2016.

[4] P. Tu, S. Member, S. Yang, and S. Member, "Reliability- and cost-based redundancy design for modular multilevel converter," *IEEE Trans. Ind. Electron.*, vol. 66, no. 3, pp. 2333–2342, Jan. 2019.

[5] Military handbook MIL-HDBK-217F: reliability prediction of electronic equipment. Washington, DC, USA, 1995.

[6] R. Faraji, L. Ding, T. Rahimi, and M. Kheshti, "Application of soft-switching cell with inherent redundancy properties for enhancing the reliability of boost-based DC-DC converters," *IEEE Trans. Power Electron.*, early access, May 2021.

[7] S. E. De Leon-Aldaco, H. Calleja, and J. Aguayo Alquicira, "Reliability and mission profiles of photovoltaic systems: a FIDES approach," *IEEE Trans. Power Electron.*, vol. 30, no. 5, pp. 2578–2586, May 2015.

[8] "A methodology for components reliability, FIDES," 2010. [Online]. Available: https://www.fides-reliability.org/. [Accessed: 11-Nov-2019].

[9] S. Peyghami, P. Palensky, and F. Blaabjerg, "An overview on the reliability of modern power electronic based power systems," *IEEE Open J. Power Electron.*, vol. 1, pp. 34–50, Feb. 2020.

[10] S. Peyghami, Z. Wang, and F. Blaabjerg, "A guideline for reliability prediction in Power Electronic converters," *IEEE Trans. Power Electron.*, vol. 35, no. 10, pp. 10958–10968, Oct. 2020.

[11] T. Dragicevic, P. Wheeler, and F. Blaabjerg, "Artificial intelligence aided automated design for reliability of power electronic systems," *IEEE Trans. Power Electron.*, vol. 34, no. 8, pp. 7161–7171, Aug. 2019.

[12] K. Ma, U. M. Choi, and F. Blaabjerg, "Prediction and validation of wear-out reliability metrics for power semiconductor devices with mission profiles in motor drive application," *IEEE Trans. Power Electron.*, vol. 33, no. 11, pp. 9843–9853, Nov. 2018.

[13] J. M. Morales, R. Mínguez, and A. J. Conejo, "A methodology to generate statistically dependent wind speed scenarios," *Appl. Energy*, vol. 87, no. 3, pp. 843–855, Mar. 2010.

[14] Y. Chen, Y. Wang, D. Kirschen, and B. Zhang, "Model-free renewable scenario generation using Generative Adversarial Networks," *IEEE Trans. Power Syst.*, vol. 33, no. 3, pp. 3265–3275, May 2018.

[15] P. Jirutitijaroen and C. Singh, "Comparison of simulation methods for power system reliability indexes and their distributions," *IEEE Trans. Power Syst.*, vol. 23, no. 2, pp. 486–493, May 2008.

[16] I. Goodfellow et al., "Generative adversarial networks," Commun. ACM, vol. 63, no. 11, pp. 139–144, Oct. 2020.

[17] S. Peyghami, F. Blaabjerg, and P. Palensky, "Incorporating power electronic converters reliability into modern power system reliability analysis," *IEEE J. Emerg. Sel. Top. Power Electron.*, pp. 1668–1681, Jan. 2020.

[18] A. Wintrich, N. Ulrich, T. Werner, and T. Reimann, Application Manual Power Semiconductors. Ilmenau, Germany: SEMIKRON International GmbH, 2015.

[19] A. Davoodi, S. Peyghami, Y. Yang, T. Dragicevic, and F. Blaabjerg, "Modelling and analysis of the reliability of a PhotoVoltaic (PV) inverter," in Proc. of Power Electronics for Distributed Generation Systems (PEDG), 2020, pp. 297–303.

[20] “Infineon AN2019-05: PC and TC Diagrams,” Munich, Germany: Infineon Technologies AG, 2019, pp. 1–15.

[21] H. Wang et al., “Transitioning to physics-of-failure as a reliability driver in power electronics,” *IEEE J. Emerg. Sel. Top. Power Electron.*, vol. 2, no. 1, pp. 97–114, Mar. 2014.

[22] M. Arjovsky, S. Chintala, and L. Bottou, “Wasserstein generative adversarial networks,” 34th Int. Conf. Mach. Learn. ICML 2017, vol. 1, pp. 298–321, 2017.

[23] L. L. . Effective Solar Products, “High-efficiency photovoltaic module using Silicon Nitride coated multicrystalline Silicon cells.” [Online]. Available: http://www.effectivesolar.com/PDF/bp/BP365.pdf. [Accessed: 12-Sep-2019].

[24] A. Andreas and T. Stoffel, “NREL Report No. DA-5500-56509,” University of Nevada (UNLV), Las Vegas, Nevada, 2006.